NANO LETTERS

pubs.acs.org/NanoLett

Near-Field Localization in Plasmonic Superfocusing: A Nanoemitter on a Tip

Catalin C. Neacsu,[†,#] Samuel Berweger,[†,#] Robert L. Olmon,[†,‡,#] Laxmikant V. Saraf,[||] Claus Ropers,[⊥] and Markus B. Raschke*[,†,§]

[†]Department of Chemistry, [‡]Department of Electrical Engineering, [§]Department of Physics, University of Washington, Seattle, Washington 98195, [||]Environmental Molecular Sciences Laboratory, Pacific Northwest National Laboratory, Richland, Washington 99352, and [⊥]Courant Research Center Nano-Spectroscopy and X-ray Imaging, University of Göttingen, Germany

ABSTRACT Focusing light to subwavelength dimensions has been a long-standing desire in optics but has remained challenging, even with new strategies based on near-field effects, polaritons, and metamaterials. The adiabatic propagation of surface plasmon polaritons (SPP) on a conical taper as proposed theoretically has recently emerged as particularly promising to obtain a nanoconfined light source at the tip. Employing grating-coupling of SPPs onto gold tips, we demonstrate plasmonic nanofocusing into a localized excitation of ~20 nm in size and investigate its near- and far-field behavior. For cone angles of ~10−20°, the breakdown of the adiabatic propagation conditions is found to be localized at or near the apex region with ~10 nm radius. Despite an asymmetric side-on SPP excitation, the apex far-field emission with axial polarization characteristics representing a radially symmetric SPP mode in the nanofocus confirms that the conical tip acts as an effective mode filter with only the fundamental radially symmetric TM mode ($m = 0$) propagating to the apex. We demonstrate the use of these tips as a source for nearly background-free scattering-type scanning near-field optical microscopy (s-SNOM).

KEYWORDS Surface plasmon polariton, near-field microscopy, nano-focusing, local-field enhacement

Nanometer-sized light sources exist in many forms, including molecules, clusters, semiconductor quantum dots, and metallic nanoparticles. Under optical excitation, the effective funneling of light energy into such emitters is fundamentally limited by the respective intrinsic scattering or absorption cross sections. In order to overcome the resulting low signal transduction and mode mismatch in optical coupling, antenna concepts may be employed.[1,2] Taking advantage of the radiationless energy transport and spatial field confinement properties of SPPs allows for SPP focusing in wedges,[3,4] tetrahedrons,[5] grooves,[6] and tapered waveguides.[7,8] Metamaterials based on nanocomposites provide another avenue for projection of a far-field source to the nanoscale.[9−13]

Despite these promising concepts, several issues persist limiting the device performances for various reasons. Guiding structures based on metamaterials are known to be vulnerable to energy attenuation through absorption losses and reflections.[10,14] Leakage radiation of SPPs contributes to loss in systems with thin conductive films or plasmonic particles atop a dielectric.[15,16] Likewise, SPP scattering from geometric inhomogeneities and defects, for example, edges or corners, inevitable in 2D geometries, gives rise to additional extrinsic damping.[17,18]

Thus the use of a monolithic noble metal structure provides several advantages, allowing for the minimization of losses as well as eliminating the need to optimize coupling between material interfaces.[19,20] Specifically, the semi-infinite conical structure provides a unique topology, possessing a high curvature (quasi-singularity) only at the apex. The propagation of SPPs along such a tapered tip has originally been proposed to result in superfocusing[21] and adiabatic energy concentration at the tip.[22,23] In theory, as the cone radius decreases to zero, the resulting divergence of the surface index of the fundamental TM mode ($m = 0$) results in both the phase and group velocities of the propagating SPP wave vanishing toward the apex. The associated adiabatic focusing and decrease in SPP wavelength prevents radiative emission (scattering), thus resulting in a nanoconfined light source at the apex. In contrast, the higher order modes ($m \neq 0$) experience a cutoff at a cone radius before reaching the apex, preventing their focusing.[24,7] However, recent theoretical results suggest that an increase in damping and the probable failure of the adiabatic conditions near the apex may limit the nanofocusing efficiency and lead to far-field emission.[25,26]

The plasmon emission characteristics and the spatial extent of the nanoconfinement at the apex of a plasmonic nanofocusing structure has not yet been determined. Having previously demonstrated the grating-coupling, propagation, and apex emission of SPP's on Au metal tips,[27] here we characterize the degree of optical nanoconfinement enabled by this geometry and show its

* To whom correspondence should be addressed. Telephone: 206-543-2906. Fax: 206-685-8665. E-mail: raschke@chem.washington.edu.

[#] These authors contributed equally to this work.

Received for review: 10/25/2009
Published on Web: 01/12/2010

DOI: 10.1021/nl903574a | *Nano Lett.* **2010,** *10,* 592-596

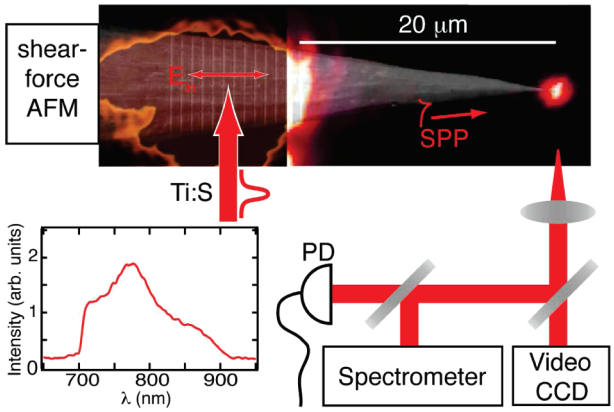

FIGURE 1. Grating coupling of surface plasmons on a tip. Overlay of SEM and optical far-field image of a Au tip with grating written by FIB for surface plasmon coupling of incident near-IR light from a Ti:Sapphire laser (spectrum shown). The grating with period $a_0 \sim$ 770 nm is illuminated with polarization parallel with respect to the tip axis and an incident focus size of $\sim$8 μm. The nonradiative SPP propagation leads to energy transfer and focusing and finally reemission near the tip apex with radius $\lesssim$15 nm.

potential for nearly background-free near-field imaging. Capable of generating a localized excitation ~20 nm in size at an apex region of ~10 nm radius, the excitation efficiency at the apex is estimated to be >100 times greater than what could be achieved with direct apex illumination under identical conditions. In addition, through characterization of the polarization of the apex emitted light we confirm of SPP mode filtering in nanoscopic noble metal tips.

For our experiment excitation of propagating SPPs onto the tip by free space optical radiation is achieved by grating coupling to overcome the momentum mismatch between the incident wavevector $k_{in,z}$ and the in-plane SPP momentum $k_{SP,z} = k_{in,z} + \nu G$ with reciprocal lattice vector $G = 2\pi/a_0$, lattice constant a_0 of the grating, and integer ν.[15] Efficient SPP propagation requires tips of homogeneous taper and a smooth surface. The tips are prepared from Au wires (diameter D = 125 μm) by electrochemical etching as described previously.[28] For the near-field imaging experiments, the tips are mounted onto a quartz tuning fork for shear-force control of the tip−sample distance, with piezo stages for both tip and sample manipulation.

Figure 1 shows the schematic of the experiment and a typical result for SPP grating coupling, evanescent plasmon propagation along the taper and their subsequent focusing with the tip imaged in a far-field microscope configuration. We utilize spatial filtering in a confocal geometry to suppress the grating-scattered illuminating light. The tip−apex emission is imaged using a video charge coupled device (CCD), or detected using either a N_2(l) cooled CCD or photodiode.

A broadband femtosecond Ti:Sapphire oscillator (Femtolasers Synergy with pulse duration $\tau \simeq 9.5$ fs, center wavelength 780 nm, spectral width ~ 130 nm) serves as a light source incident normal with respect to the surface of the grating. As predicted theoretically,[25] a large field enhancement at the apex is expected at this wavelength for the cone angles used (~10−20°). Gratings with $a_0 \simeq 770$ nm were fabricated by focused ion beam (FIB) milling with ~150 nm groove depth and ~100 nm in width,[27] resulting in an SPP resonance within the laser bandwidth for near normal incidence. Grating distances of 10−25 μm from the apex were chosen, guided by the trade-off between backscattering suppression and $1/e$ SPP propagation length L in the near-IR spectral range with $L = (c/\omega)[(\epsilon'_m + 1)^3\epsilon'_m]^{1/2}/\epsilon''_m$, with free-space frequency ω, and permittivity $\epsilon_m = \epsilon'_m + i\epsilon''_m \simeq -23 + 1.5i$ for Au at 800 nm. For our excitation energy and material parameters,[29] $L \simeq 40$ μm.

Associated with the breakdown of the adiabatic propagation conditions near the tip, nonradiative reflection, absorptive losses, and far-field emission occur. The induced polarization across the grating structure is responsible for launching a transverse magnetic SPP wave with both transverse and longitudinal electric field components. Optical emission from the tip is observed only for an incident polarization parallel with respect to the tip axis, as expected.[15]

As shown previously,[27] the characteristics of the emission from the apex are qualitatively distinct from the light scattering observed in direct dark field apex illumination and detection. For direct illumination, despite local field enhancement at the apex, due to the increase in polarizable tip volume away from the apex, the highest scattering efficiency observed does not correspond to the apex position. In contrast, for the grating-mediated SPP excitation a diffraction limited emission from the tip apex is observed (Figure 1), as is evident from the point spread function centered at the geometric apex position.

Figure 2 shows the polarization and spectrally resolved characterization of the grating-mediated tip apex emission after spatial filtering for orthogonal grating illumination and scattering detection. The center wavelength for resonant emission is seen at 740 nm with typical values ranging between 730 and 750 nm. This shift to shorter wavelengths compared with the design wavelength (780 nm for a grating period of $a_0 \sim 770$ nm) can be attributed to deviations of the angles of incidence from the surface normal on the structure. First, rapid resonance shifts (nearly linear with angle with ~10 nm per degree) are expected for slight tilt in the plane formed by tip axis and incident k-vector. Second, the excitation on the curved cone surface leads to a broad distribution of angles of incidence in the plane perpendicular to the tip axis and parallel to the grooves. The associated resonance shifts scale quadratically with angle of incidence and due to the significant curvature across the grating this also contributes to the observed blue-shift.

The observed value of 25 nm full-width at half-maximum (fwhm) is spectrally considerably narrower than what one would expect from the estimate of the spatial Fourier transform of the illuminated grating. With the corresponding relationship for the inverse of the coupling bandwidth $\Delta G \geq 2\pi/a_0 n$, where n is the number of illuminated grooves,

DOI: 10.1021/nl903574a | Nano Lett. 2010, 10, 592-596

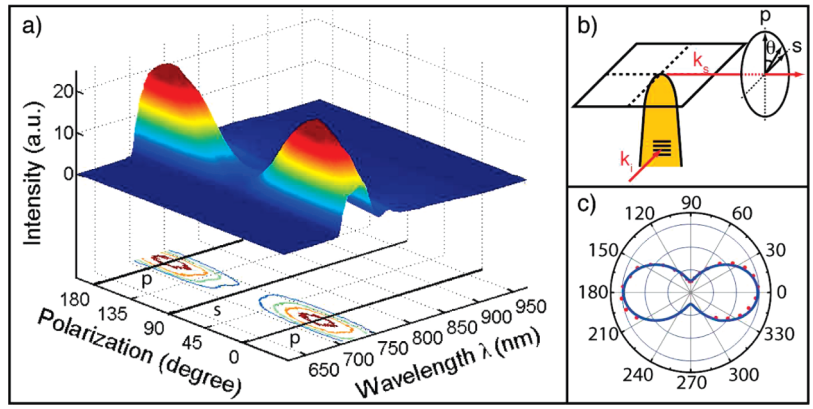

FIGURE 2. Point dipole emission of nanosource on tip. Spectrally resolved (a) and intensity integrated (c) polarization anisotropy of tip apex emission as measured under the scattering configuration in (b). The numerical fit in (c) with $I(\theta) = I_0 + A\cos^2(\theta)$ corresponding to a dipolar polarization characteristic is indicative of a subwavelength size Rayleigh emitter. A weak isotropic background to the tip emission gives rise to the small signal offset I_0.

the estimated free-space fwhm for 10 grooves would be $\Delta\lambda = 94$ nm. The discrepancy is possibly due to the fact that in addition to the number of grooves, a complex phase dependent superposition of the local modes excited within the grooves and at the ridges influence the spectral coupling bandwidth.[30,31]

The symmetric 2-fold polarization anisotropy observed can be described by an emission pattern following $I(\theta) = I_0 + A\cos^2(\theta)$ as shown by the numerical fit of the spectrally integrated data corresponding to a longitudinal polarization of the emitter. With $A/I_0 \simeq 5.5$, this behavior is characteristic for a Rayleigh dipole of subwavelength dimensions oriented along the tip axial direction with a weak isotropically polarized background originating primarily from residual grating scattering.

The determination of the size of an optical emitter of subwavelength dimensions is possible, in general, by probing the spatial extent of its optical near-field by scanning a scattering probe smaller than the emitter size across its surface. This approach of scattering-scanning near-field optical microscopy (s-SNOM) allows for spatial mapping of plasmonic near-field modes with nanometer spatial resolution.[32,33] Here, we utilize an inverse s-SNOM scheme, scanning the nanofocusing tip across a step edge of a silicon surface as shown schematically in Figure 3a. The step edge serves as a local scattering center with a radius 3 ± 1 nm, characterized by high resolution SEM (Figure 3b). The use of Si as the sample material ensures minimal perturbation of the intrinsic tip near-field spatial distribution and its polarization due to the weak near-field dipole−dipole tip−sample coupling with low dielectric constants for Si and SiO_2 in the visible.[34]

With a step wall angle of $\sim 60°$, the tip shaft (cone angle 14°) does not touch the step edge, thus avoiding possible distortions of the plasmon propagation along the shaft during scanning. As the tip traverses the scattering edge, enhanced emission from the apex is observed (Figure 3c) with a fwhm of the signal of 22 ± 5 nm. The lateral width of this enhancement provides a measure of the spatial extent

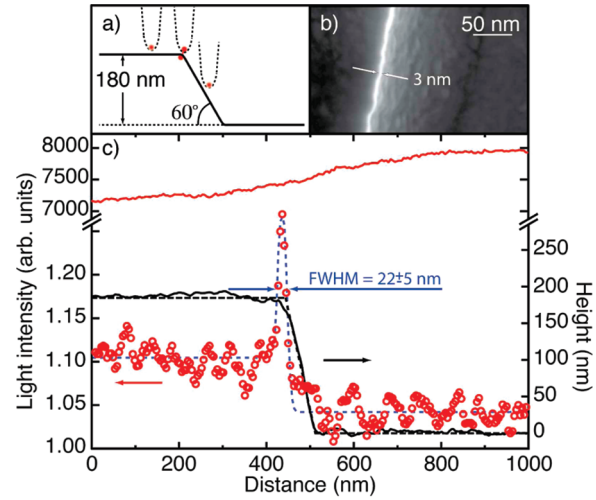

FIGURE 3. Determination of tip emitter size. (a) Schematic of scanning the nanofocusing tip across a silicon step edge with radius 3 ± 1 nm. (b) Top view SEM image of step edge. The wall and lower terrace are on the right-hand side. The edge serves as a local scatterer of the optical near-field of the apex. (c) The optical signal of a lateral scan across the step edge provides a measure of the spatial field confinement and thus the emitter size at the apex. Solid black line: AFM topography of the step. Red circles: plasmonic edge-scattered light intensity of the apex. The optical intensity peaks at the step edge and displays a width of 22 ± 5 nm, demonstrating the near-field localization at the apex. Solid red: Signal obtained under direct illumination of the apex under otherwise identical conditions.

of the apex confined field. From a simple model deconvolution considering a tip at 5 nm above the surface, the fwhm of the signal observed corresponds to a spatial confinement of the nanofocused field to the apex region with radius of only $r \simeq 10$ nm

Specifically, the emission observed arises from redistribution among the three main SPP loss channels at the apex, namely absorption, SPP reflection, and scattering into the far-field. In the case of metallic samples, the additional coupling into SPPs on the surface would need to be considered. In the present case, the enhanced local sample polar-

DOI: 10.1021/nl903574a | *Nano Lett.* **2010,** *10,* 592-596

izability at the step edge results in a stronger coupling of the near-field into far-field radiation.[34]

The slightly different signal levels with the tip on the upper and lower sample terraces are due to far-field interference of the apex emission E_{tip} with a small residual background field from sample reflected scattered light of the grating E_g^{scat}, with effective distance d dependent phase $\Phi(d)$ which affects the intensity as $|E_{tip} + E_g^{scat} e^{i\Phi(d)}|^2$.

It should be noted that the tip-scattered signal is detected without any tip−sample modulation. This fundamentally different performance becomes particularly evident when comparing to a corresponding line scan performed under direct apex illumination instead of the grating coupling. The upper trace in Figure 3c (solid red line) shows that signal trace under otherwise identical conditions. Although a field enhancement and spatial confinement by the tip apex is expected, the corresponding edge scattered signal is not discernible, as it is overwhelmed by the 3 orders of magnitude more intense far-field scattering of the tip shaft and sample. Related to this performance is the application of the grating coupled tips for the otherwise difficult task of nearly background-free near-field imaging (see Supporting Information).

The basis of the nanofocusing observed, as theoretically suggested before, is that the effective wavelength of the fundamental TM surface wave on a cylindrical wire decreases with decreasing wire diameter.[21,22,25,24,7] This can be expressed by λ/n_{eff}, with n_{eff} the effective refractive index increasing sharply with decreasing wire radius below 0.1λ.[25] This effect avoids diffraction and enables the continuous focusing with a concurrent increase in local field energy. The process proceeds adiabatically, provided that the tip tapers gradually as compared to the effective SPP wavelength, thus avoiding waveguide cutoff and associated reflection or radiative emission. However, as understood from theoretical investigations, with the shorter wavelength and the concomitant decrease in group velocity of the propagating SPP, the damping is expected to rise appreciably.[25,26] Consequently, as the group velocity asymptotically tends to zero, despite the absence of reflection, the SPP dissipation into heat will lead to a decrease in field energy as the SPP approaches the tip. While a larger taper angle would result in a shorter propagation distance, thus reducing loss, the breakdown of the adiabatic conditions, however, is expected to occur at larger distances from the apex, thus limiting the nanofocusing capability. It appears, however, that it may be possible to achieve higher field enhancement under nonadiabatic conditions near the apex.[25]

Although the details depend on tip material, wavelength, taper angle, and initial wire diameter, an optimal angle between 10−40° has been suggested to achieve maximal field enhancement as a trade-off between absorptive (adiabatic condition) and radiative and reflective (nonadiabatic condition) losses.[26,25] This condition was suggested to still allow for spatial confinement at the tip with nanometer dimensions on the order of the apex radius. Our results are consistent with these model calculations, given that with cone angles of ∼10−20° the breakdown of the adiabatic propagation conditions is found to be localized near the apex region with ≳10 nm radius.

As discussed above, unlike in theoretical treatments where an initial SPP excitation of only the radially symmetric $m = 0$ TM mode has been assumed,[22,25,26,35] our asymmetric excitation is expected to generate a superposition of different normal SPP modes of the cylindrical structure ($m = 0, 1, 2,...$). As these different waves propagate toward the apex, the critical cutoff radius for all but the $m = 0$ mode of the tip is expected to prevent propagation and nanofocusing. Our emission characteristics observed, lacking a polarization component along the transverse direction, indicate a radially symmetric SPP. This provides strong evidence of mode filtering in SPP propagation and nanofocusing on tapered tips. We do note that the differing longitudinal and transverse polarizabilities due to the localized plasmon resonances of the tip enhance on-axis field components in the radiated far-field.[28]

The observed far-field radiating emission from the apex corresponds to 2−4% of the incident radiation within the coupling bandwidth. With the effective nanofocus size of ∼20 nm at the apex as shown above, the focus volume is 4 orders of magnitude smaller than what can be achieved by high numerical aperture far-field focusing (focus size ca. $\lambda/2$). With the cone angle of (∼15°) used here, the coupling wavelength of 750 nm corresponds to near-optimal conditions to deliver maximum field enhancement at the tip apex as predicted theoretically.[25] Furthermore, the narrow cone angle is expected to lead to a large degree of adiabaticity, indicating that a large evanescent near-field component of the confined SPP is expected at the tip apex. Therefore, even with a maximum loss of 96−98% due to inefficient grating coupling, SPP propagation loss, and SPP reflection near the apex, the excitation efficiency of the local apex is still ∼100 times higher compared to the best possible direct illumination. This allows for background-free tip-enhanced Raman spectroscopy.[36,37]

With a near-optimal taper angle for the wavelength used here, we expect losses due to grating coupling and mode filtering to be the limiting factors in our experiment. Through the use of radially symmetric SPP generation[35] to generate only the fundamental $m = 0$ mode, losses due to attenuation of higher order ($m \neq 0$) modes can be avoided. Furthermore, with grating coupling efficiency sensitively depending on groove profile, width, and depth as suggested theoretically, tip performance can thus be considerably increased with optimal grating designs[38,31] including holographic and broadband structures in combination with pulse shaping for ultrafast pulsed excitation and coherent control. As the magnitude of nanofocused energy contained in the evanescent field is unknown, our efficiency includes mode filtering losses and represents a lower limit for the $m = 0$ mode.

DOI: 10.1021/nl903574a | Nano Lett. 2010, 10, 592-596

Through suitable optimization, predicted absolute efficiencies of >50 %[7] may be achievable.

Including grating coupling, SPP propagation, and field confinement at the tip, the nanostructure as a whole acts as an optical antenna with some unique features. The propagation of a spatially distributed source polarization in the form of propagating SPPs converging into the tip apex is equivalent to the concentration of radiation in an antenna coupled detector configuration. The high field confinement provided by the grating-coupled tip, despite propagation and reflection losses, can provide an efficient excitation source of small (hence low noise) detectors, analyte molecules, or nanoscale waveguides.

In summary, our experiments demonstrate the experimental realization of optical nanofocusing on a conical tip. The breakdown of the adiabtic conditions is found to occur only within the last 10s of nanometers, as determined by the tip apex radius which lends strong support to the theoretically proposed mechanisms. Despite the symmetry-breaking side-on illumination and a resulting SPP excitation confined along the azimuth, the tip effectively acts as a mode filter, giving rise to a propagation-induced, nanoscopic SPP excitation with radial symmetry at the apex. This result demonstrates the robustness of conical SPP focusing with respect to asymmetries and imperfections in the SPP generation. The resulting dipolar nanoemitter with ~20 nm spatial confinement, that is, more than 1 order of magnitude beyond the diffraction limit, represents a novel light source which we expect to find numerous applications, such as new forms of field-enhanced microscopy or other forms of antenna-based sensing, nonlinear frequency mixing including higher harmonics generation,[39] attosecond XUV generation, and photoelectron microscopy.[40,41]

Acknowledgment. Funding from the National Science Foundation (NSF CAREER Grant CHE0748226 and NSF-IGERT program) is greatly acknowledged. A part of the research was performed using EMSL, a national scientific user facility sponsored by the Department of Energy's Office of Biological and Environmental Research and located at Pacific Northwest National Laboratory. C.R. gratefully acknowledges funding from the German Excellence Initiative (FL3).

Supporting Information Available. This material is available free of charge via the Internet at http://pubs.acs.org.

REFERENCES AND NOTES

(1) Akimov, A. V.; Mukherjee, A.; Yu, C. L.; Chang, D. E.; Zibrov, A. S.; Hemmer, P. R.; Park, H.; Lukin, M. D. *Nature* **2007**, *450*, 402.
(2) Ditlbacher, H.; Hohenau, A.; Wagner, D.; Kreibig, U.; Rogers, M.; Hofer, F.; Aussenegg, F. R.; Krenn, J. R. *Phys. Rev. Lett.* **2005**, *95*, 257403.
(3) Durach, M.; Rusina, A.; Stockman, M. I.; Nelson, K. *Nano Lett.* **2007**, *7*, 3145.
(4) Lapchuk, A. S.; Shylo, S. A.; Nevirkovets, I. P. *J. Opt. Soc. Am. A* **2008**, *25*, 1535.
(5) Tanaka, K.; Burr, G.; Grosjean, T.; Maletzky, T.; Fischer, U. *Appl. Phys. B* **2008**, *93*, 257.
(6) Volkov, V. S.; Bozhevolnyi, S. I.; Rodrigo, S. G.; Martín-Moreno, L.; García-Vidal, F. J.; Devaux, E.; Ebbesen, T. W. *Nano Lett.* **2009**, *9*, 1278.
(7) Verhagen, E.; Spasenovic, M.; Polman, A.; (Kobus) Kuipers, L. *Phys. Rev. Lett.* **2009**, *102*, 203904.
(8) Maier, S. A.; Andrews, S. R.; Martin-Moreno, L.; Garcia-Vidal, F. J. *Phys. Rev. Lett.* **2006**, *97*, 176805.
(9) Elser, J.; Govyadinov, A. A.; Avrutsky, I.; Salakhutdinov, I.; Podolskiy, V. A. *J. Nanomater.* **2007**, *2007*, 79469–79477.
(10) Govyadinov, A. A.; Podolskiy, V. A. *Phys. Rev. B* **2006**, *73*, 155108.
(11) Liu, Z.; Lee, H.; Xiong, Y.; Sun, C.; Zhang, X. *Science* **2007**, *315*, 1686.
(12) Pendry, J. B. *Phys. Rev. Lett.* **2000**, *85*, 3966.
(13) Cubukcu, E.; Aydin, K.; Ozbay, E.; Foteinopolou, S.; Soukoulis, C. M. *Phys. Rev. Lett.* **2003**, *91*, 207401.
(14) Smith, D. R.; Schurig, D.; Rosenbluth, M.; Schultz, S.; Ramakrishna, S. A.; Pendry, J. B. *Appl. Phys. Lett.* **2003**, *82*, 1506.
(15) Raether, H. *Surface plasmons on smooth and rough surfaces and on gratings*; Springer-Verlag: 1988.
(16) Drezet, A.; Hohenau, A.; Koller, D.; Stepanov, A.; Ditlbacher, H.; Steinberger, B.; Aussenegg, F.; Leitner, A.; Krenn, J. *Mater. Sci. Eng., B* **2008**, *149*, 220.
(17) Elser, J.; Podolskiy, V. A. *Phys. Rev. Lett.* **2008**, *100*, 066402.
(18) Oulton, R. F.; Pile, D. F. P.; Liu, Y.; Zhang, X. *Phys. Rev. B* **2007**, *76*, 035408.
(19) Chen, X.-W.; Sandoghdar, V.; Agio, M. *Nano Lett.* **2009**, *9*, 3756.
(20) De Angelis, F.; Patrini, M.; Das, G.; Maksymov, I.; Galli, M.; Businaro, L.; Andreani, L. C.; Di Fabrizio, E. *Nano Lett.* **2008**, *8*, 2312.
(21) Babadjanyan, A. J.; Margaryan, N. L.; Nerkararyan, K. V. *J. Appl. Phys.* **2000**, *87*, 3785.
(22) Stockman, M. I. *Phys. Rev. Lett.* **2004**, *93*, 137404.
(23) Ruppin, R. *Phys. Lett. A* **2005**, *340*, 299.
(24) Chang, D. E.; Sorensen, A. S.; Hemmer, P. R.; Lukin, M. D. *Phys. Rev. Lett.* **2006**, *97*, 053002.
(25) Issa, N.; Guckenberger, R. *Plasmonics* **2007**, *2*, 31.
(26) Gramotnev, D. K.; Vogel, M. W.; Stockman, M. I. *J. Appl. Phys.* **2008**, *104*, 034311.
(27) Ropers, C.; Neacsu, C. C.; Elsaesser, T.; Albrecht, M.; Raschke, M. B.; Lienau, C. *Nano Lett.* **2007**, *7*, 2784.
(28) Neacsu, C. C.; Steudle, G. A.; Raschke, M. B. *Appl. Phys. B* **2005**, *80*, 295.
(29) Johnson, P. B.; Christy, R. W. *Phys. Rev. B* **1972**, *6*, 4370.
(30) Ditlbacher, H.; Krenn, J. R.; Hohenau, A.; Leitner, A.; Aussenegg, F. R. *Appl. Phys. Lett.* **2003**, *83*, 3665.
(31) Renger, J.; Grafstrom, S.; Eng, L. M. *Phys. Rev. B* **2007**, *76*, 045431.
(32) Rang, M.; Jones, A. C.; Zhou, F.; Li, Z.-Y.; Wiley, B. J.; Xia, Y.; Raschke, M. B. *Nano Lett.* **2008**, *8*, 3357.
(33) Hillenbrand, R.; Keilmann, F.; Hanarp, P.; Sutherland, D. S.; Aizpurua, J. *Appl. Phys. Lett.* **2003**, *83*, 368.
(34) Raschke, M. B.; Lienau, C. *Appl. Phys. Lett.* **2003**, *83*, 5089.
(35) Baida, F.; Belkhir, A. *Plasmonics* **2009**, *4*, 51.
(36) Berweger, S.; Olmon, R. L.; Raschke, M. B. Unpublished work, 2009.
(37) De Angelis, F.; Das, G.; Candeloro, P.; Patrini, M.; Galli, M.; Bek, A.; Lazzarino, M.; Maksiymov, I.; Liberale, C.; Andreani, L. C.; et al. *Nat. Nanotechnol.* **2009**, *5*, 67.
(38) Leveque, G.; Martin, O. J. F. *J. Appl. Phys.* **2006**, *100*, 124301.
(39) Stockman, M. I.; Kling, M. F.; Kleineberg, U.; Krausz, F. *Nat. Photon.* **2007**, *1*, 539.
(40) Ropers, C.; Solli, D. R.; Schulz, C. P.; Lienau, C.; Elsaesser, T. *Phys. Rev. Lett.* **2007**, *98*, 043907.
(41) Kubo, A.; Pontius, N.; Petek, H. *Nano Lett.* **2007**, *7*, 470.

DOI: 10.1021/nl903574a | *Nano Lett.* **2010,** *10,* 592-596